Construction and Building Materials 223 (2019) 806–816

Contents lists available at ScienceDirect

Construction and Building Materials

journal homepage: www.elsevier.com/locate/conbuildmat

Numerical prediction of effective diffusivity in hardened cement paste between aggregates using different shapes of cement powder

Cheng Liu [a], Chen Qian [b], Rusheng Qian [a], Zhiyong Liu [a,*], Hongxia Qiao [c], Yunsheng Zhang [c]

[a] Jiangsu Key Laboratory for Construction Materials, School of Materials Science and Engineering, Southeast University, Nanjing 211189, China
[b] Biostatistics and Bioinformatics Facility, James Graham Brown Cancer Center, University of Louisville, Louisville KY 40202, USA
[c] School of Civil Engineering, Lanzhou University of Technology, Lanzhou 730050, China

HIGHLIGHTS

- Accuracy for predicting diffusivity using spherical cement particles is studied.
- A random walk method for two-component random-diffusive mixture is proposed.
- Diffusivity simulated using spherical cement is overestimated by 0–40%.
- Overestimation is due to initial shape of cement, capillary pore and C-S-H morphology.

ARTICLE INFO

Article history:
Received 6 March 2019
Received in revised form 8 June 2019
Accepted 15 June 2019
Available online 13 July 2019

Keywords:
Diffusivity
Irregular-shaped cement powder
Spherical
Microstructure
Hydration
Modelling

ABSTRACT

The numerical prediction of effective diffusivity in hardened cement paste has been a hot point in the past few decades. However, the shape of cement powder is normally over-simplified as sphere in most models, which may influence the accuracy of prediction. To assess this effect of the shaped simplification on the prediction of effective diffusivity in cement paste, a microstructure-based model considering irregular-shaped cement powders that are close to the real one, and spherical cement powder respectively, is presented to simulate the hydrating cement pastes between aggregates (interfacial transition zone and bulk cement paste) and predict their effective diffusivities. The results indicate that the effect of the shape of cement powder on the distributions of capillary pore and unhydrated cement is weak. Furthermore, compared to the irregular-shaped cement powder, the diffusivity in cement paste simulated using spherical cement powders is overestimated by 0–40%. It is ascribed to three discrepancies, i.e., the shape of initial cement powder, the formation of capillary pore structure, and the morphology of C-S-H. However, the predicting error using spherical cement powder is still acceptable by contrast to the large difference of diffusivity in hardened cement paste with cement hydration, i.e., normally two orders of magnitude difference between early and later curing ages.

1. Introduction

The chemical degradation of concrete structure is ascribed to the ingress of aggressive agents (e.g., water, harmful ions and aggressive gases) into cementitious materials. As a result, transport properties are normally regarded as indicators of durability estimation of concrete. One of the most important transport properties is diffusivity which is widely used for the service life prediction models of reinforced concrete structure, e.g., Duracrete [1]. The diffusivity in cementitious materials can be measured using the natural diffusion test and the electrically accelerated test [2]. Unfortunately, due to the less penetration of cementitious materials, it is far from being a trivial task to measure diffusivity in cementitious materials besides the time-consuming and prohibitive experimental procedure. To overcome these drawbacks, the prediction of diffusivity in cementitious materials has been a popular point in the past few decades. The models for predicting diffusivity of cementitious materials are mainly classified into three groups, i.e., empirical models, analytical or theoretical models, and numerical or computer-based models [2]. Compared to empirical models and analytical models, numerical models hold great advantages. For example, numerical models can hold the sufficient accuracy as the volume fractions of dispersed components

* Corresponding author at: Jiangsu Key Laboratory for Construction Materials, School of Materials Science and Engineering, Southeast University, Nanjing 211189, China.
E-mail address: liuzhiyong0728@163.com (Z. Liu).

https://doi.org/10.1016/j.conbuildmat.2019.06.125
0950-0618/

are very high or large contrast in constituent properties exists [3–5], as well as be applied to the complex microstructures of cementitious materials.

To predict the diffusivity in hardened cement paste, numerous numerical methods based on various cement hydration models, i.e., CEMHYD3D [6] and HYMOSTRUC3D [7], together with different numerical solvers for the mass diffusion equation, i.e., finite difference method (FDM), finite element method (FEM), lattice Boltzmann method (LBM) and random walk method (RWM), were proposed. Using the simulated cement paste obtained from CEMHYD3D, Garboczi and Bentz [8] developed FDM- and FEM-based models to calculate the effective diffusivity of hardened cement paste at various water-to-cement (w/c) ratios and degrees of hydration (DOHs). They proposed a semi-empirical equation related to the capillary porosity of cement paste

$$\frac{D_e}{D_0} = 0.001 + 0.07\phi_c + H(\phi_c - 0.18) \times 1.8 \times (\phi_c - 0.18)^2 \quad (1)$$

where ϕ_c is the capillary porosity, H is the Heavy-side step function, $H(\phi_c - 0.18) = 0$ for $(\phi_c - 0.18) < 0$, $H(\phi_c - 0.18) = 1$ for $(\phi_c - 0.18) > 0$ and 0.18 is defined as the percolation threshold of the capillary pore space of cement paste. Afterwards, Kamali-Bernard et al. [9] and Yang and Wang [10] respectively used FEM and LBM to predict diffusivity in hardened cement pastes simulated using CEMHYD3D. In terms of HYMOSTRUC3D platform, Zhang et al. [11,12] estimated the diffusivity in virtual cement paste at various w/c ratios, DOHs and degrees of water saturation using FEM and LBM. Similarly, Ukrainczyk and Koenders [13] calculated the diffusivity of cement paste using FDM. Alternatively, Liu et al. [14] used RWM to record the relationship between displacement and time steps of a large number of walkers in capillary pores and calculated the diffusivity based on the Einstein–Smoluchowski equation. The predicting accuracy of diffusivity in cement paste is affected by the numerical solvers and the morphology of simulated cement paste. Nevertheless, it was reported that as using the same cement paste simulated by HYMOSTRUC3D, the predicting diffusivities are close to each other regardless of the numerical solvers, e.g., FEM and RWM [14]. As a result, the predictive accuracy of diffusivity mainly depends on the morpholohy of virtual microstructure of cement paste.

In the models above cited, the initial cement powder shapes are all approximated by sphere for simplicity to simulate microstructure of cement paste, though cement micrographs indicate cement particles are irregular. Our previous publications [15,16] have demonstrated that the cement powder shapes significantly affect the hydration process and microstructural evolution of cement paste using simulated irregular-shaped cement powders. This finding has been also confirmed by Bullard and Garboczi [17] and Chen et al. [18] using real-shaped and non-spherical regular cement. Nevertheless, the effect of over-simplified cement powders on predicted properties of hardened cement paste has not been considered. In the hardened cement paste, the species diffuse through pore space which is classified into capillary pore and gel pore in calcium silicate hydrate (C-S-H). The contribution of dominate pore to diffusion can be distinguished using capillary pore percolation. Before capillary pore reaches percolation, capillary pore serves as the main diffusive channel, by contrast, gel pore in C-S-H forms the main diffusive pathway after capillary pore depercolates [19]. The prediction of diffusivity in cement paste is dependent on the capillary pore structure as well as the C-S-H structure in simulated cement paste. The mentioned capillary pore structure and the C-S-H structure are influenced by the initial shape of cement powder. Therefore, the scope of this study is to assess the effect of the simplification of initial shape of cement powder on the prediction of effective diffusivity in hardened cement paste.

To this end, a microstructure-based model considering irregular-shaped cement powders that are close to the real one, and spherical cement powder, is presented to simulate the hydrating cement pastes between aggregates (interfacial transition zone and bulk cement paste) and predict their effective diffusivity. The modelling results obtained using irregular-shaped cement powders are compared to that from spherical cement powders. As such, this paper is organized as follows: in Section 2, the modelling procedure of cement paste between aggregates is presented. The hydrating cement pastes are simulated using CEMHYD3D model in which the shape of cement powder is close to the real one and spherical one, respectively. After obtaining the hydrating cement paste, in Section 3, a random walk method for the two-component random-diffusive mixture is proposed to calculate the effective diffusivity in cement paste. In Section 4, the outcomes simulated using irregular-shaped and spherical cement powders are presented and compared with each other. Herein, the diffusivities in cement pastes at three water-to-cement ratios, i.e., 0.30, 0.40 and 0.50, with various degrees of hydration, are predicted. The reasons regarding the discrepancy of simulated diffusivity in cement paste are discussed. Finally, the conclusions are presented in Section 5.

2. Modelling hydration of cement paste between aggregates

It is well recognized that the hydration process of cement pastes in mortar or concrete is different from that of neat cement pastes due to the aggregate-induced wall effect. As mixed with aggregate in size of millimetre- or centimetre-scale, the packing of cement particles in size of micrometer-scale can be disrupted, which leads to that small cement particles pack more easily in the vicinity of aggregate surface compared to larger ones [20]. This effect leading to disrupted packing is named wall effect which is the reason for the formation of interfacial transition zone. As a result, the cement pastes between aggregates are normally classified into bulk cement paste (BCP) and interfacial transition zone (ITZ). To model the wall effect, numerous sophisticated numerical cement hydration models are extended to simulate 3D microstructural development of cement pastes between aggregates. The wall effect is modelled by applying non-periodic boundary conditions on the surfaces of the representative volume element (RVE) or inserting plant aggregate in the middle of REV. These models have been performed in codes, e.g., HYMOSTRUC3D [21], SPACE [22,23] and CEMHYD3D [24]. However, the shapes of cement particles in these models are over-simply regarded as spheres. Although the real shapes of reference cement obtained from X-ray CT were employed to replace the spherical particles in specific hydration model, e.g., CEMHYD3D [17], the shaped database for cement particles are still too limited and the real shapes are only suitable for large particles due to the limitation of resolution for X-ray CT, e.g., 0.95 μm/voxel. In addition, the effect of cement particle shapes on the packing between aggregates and transport properties in cement pastes has not been fully explored.

Recently, based on hydration rules of CEMHYD3D, a modified version using simulated irregular-shaped cement powders is proposed [15]. The irregular-shaped particle is reconstructed using one pre-defined growth eigenvector which corresponds to one fixed shaped particle. The hydration process and microstructural development of neat cement paste are investigated using this modified hydration model. Consequently, we will model the microstructural evolution of ITZ and BCP using this model together with non-periodic boundary conditions. The cement pastes between aggregates are simulated as follows. Based on the known w/c ratio, the information of cement particles, e.g., quantity in each size range, is calculated following the real particle size distribution.

Herein, the diameter of irregular-shaped particles is equal to the equivalent diameter of spherical particles. The representative volume element (RVE) of cement pastes is selected to be 100 μm on each size which is demonstrated to be representative. The resolution is 0.5 μm/voxel on which the particle shape can be well reconstructed and the computational capacity is accepted for CEMHYD3D model [15]. Accordingly, the particles are thrown into the RVE from the largest one to the smallest one using the Monte Carlo simulation. The cement particles cannot overlap with each other. Fig. 1 shows a simplified structure of cement pastes between aggregates. To model the effect of aggregates on cement hydration non-periodic boundary conditions are employed in one certain dimension, while periodic boundary conditions are performed on the other two dimensions for eliminating finite size effects. In addition, for the ordinary mortars or concrete in which the aggregates account for nearly 50–60% and 60–70% of total volume, 80% and 90% of the total volume of cement pastes on average for mortar and concrete respectively lies in the vicinity of the aggregate surface within 100 μm [25]. As such, this determined RVE with 100 μm on each side is also meaningful for modelling the formation of ITZ.

After obtaining the pre-hydrated cement pastes, these structures are incorporated into CEMHYD3D to simulate cement hydration and microstructural development. It should be noted that the reason why we use CEMHYD3D is mainly due to its open-source hydration rules in spite of its obvious drawbacks, e.g., resolution-dependence [26]. The modelling procedure of hydration model contains two steps. Firstly, the packing cement particles are divided into four mineral clinkers (C_3S, C_2S, C_3A and C_4AF) based on autocorrelation functions determined by scanning electron microscopy images of the real cement powders. Afterwards, the hydration rules are carried out on the discrete structure based on the evolution of a cellular automaton. The basic chemical reactions in hydration are controlled by the sequence of dissolution, diffusion and precipitation with certain probabilities. During the evolution process, the continuous microstructural development can be obtained. The real hydration time can be determined using a fitting parameter related to the computational cycles. The detailed information of these two steps can refer to Ref. [27,28].

To understand the effect of morphology of cement powders on the structural formation and diffusive properties of BPC and ITZ respectively, the cement paste matrix is artificially separated. From the previous experiments of 2D imaging techniques combined with imaging processing, the observed outcomes demonstrated that the phase distribution shows a gradient in cement pastes between aggregates away from the aggregate surface [20,29,30]. The phase contents, e.g., capillary porosity and unhydrated cement particles, change dramatically in the vicinity of the aggregate surface, then tend to stable when reaching to the BCP. As such, the phase contents of each slice away from the aggregate surface in simulated cement pastes can be calculated. According to the characteristics of high content of capillary pores and low content of unhydrated cement particles in ITZ, the same imaging analysis in 2D can be extended on the 3D microstructure to determine ITZ structure as well as its thickness.

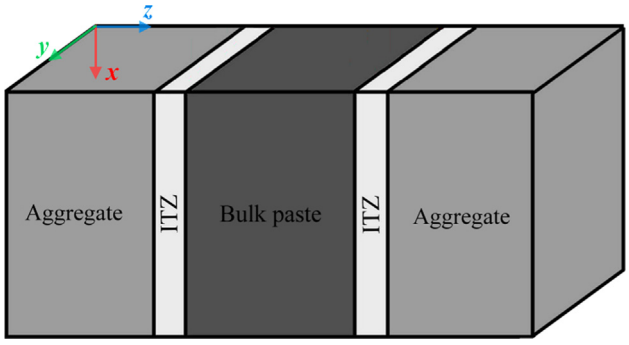

Fig. 1. Simplified structure of cement paste between aggregates.

In this study, the information of a commercial Chinese cement named P.I cement grinded by ball mill is employed as input parameters. The mineral phase compositions of this cement obtained from backscattering electron image combined with the mapping technique are 52.36% C_3S, 29.75% C_2S, 4.77% C_3A and 13.12% C_4AF respectively. The other information of P.I cement powders as input parameters of CEMHYD3D, e.g., autocorrelation functions of each mineral clinker, can be found in Ref. [15]. In terms of shaped descriptors of real cement powder, the average principle moment ratio that can indicate the geometry of objective in 3D was employed. Using X-ray computed tomography images with a resolution of 0.5 μm/voxel, the average principle moment of inertia ratio (maximum moment/minimum moment) is calculated to be around 2.0 for the P.I cement powders with size between 4 μm and 50 μm [31]. This value is similar to that of OPC CEM I 32.5R [32]. In terms of the cement particle with the size of smaller than 4 μm, the shapes were also produced using the same growth eigenvector, while it may lead to various shapes that are far away from the pre-defined one due to the limited constituent voxels. Nevertheless, the effect of small cement particles on microstructural formation is not significant since they quickly react with water at the early time. This simplification was commonly used in CEMHYD3D model due to the limited resolution [33].

3. Determination of effective diffusivity

3.1. Random walk method

In this study, a RWM for the two-component random-diffusive mixture is proposed to calculate the effective diffusivity in hardened cement paste. RWM is an algorithm to simulate the diffusion of non-sorbing species in porous materials, e.g., H_2O and Cl^-. For the classical RWM in a three-dimensional space, a random walker initially starts at the original diffusive position and moves towards its neighbouring positions with a certain probability. Starting at the original position 0, the displacement of a walker after N steps is $\vec{\boldsymbol{R}}_N = \sum_{n=1}^{N} \Delta\vec{\boldsymbol{r}}_n$, where $\Delta\vec{\boldsymbol{r}}_n\{n = 1, 2, \ldots N\}$ is an independent variable, $\left\{\vec{\boldsymbol{R}}_N\right\}$ denotes a Markov chain, referring to a set of all positions in a random walk process. According to the Markov assumption, the probability of finding a random walker at $\boldsymbol{R}$ after $N + 1$ steps is

$$P(\boldsymbol{R}, N+1) = \int p(\boldsymbol{r}')P(\boldsymbol{R}-\boldsymbol{r}', N)d\boldsymbol{r}' \tag{2}$$

where $p(\boldsymbol{r}')$ is the transition probability from state $\boldsymbol{R}(N)$ to $\boldsymbol{R}(N+1)$. As $N \to \infty$, it has been shown that the limit distribution $\delta(\boldsymbol{R}, t)$, defined by $\delta(\boldsymbol{R}, N\Delta t) = P(\boldsymbol{R}, N)$, is satisfied with the diffusion equation

$$\frac{\partial\delta}{\partial t} = D\nabla^2\delta \tag{3}$$

with the initial condition $\delta(\boldsymbol{R}, 0) = \delta_0(\boldsymbol{R})$. Herein, let the mean square displacement of a walker be $R_N^2 = \vec{\boldsymbol{R}}_N \cdot \vec{\boldsymbol{R}}_N$ and the travelling time of the walker be t_N after N steps. Eq. (3) can be written as

$$D = \frac{\left\langle R_N^2 \right\rangle}{2dt_N} \tag{4}$$

which means that the mean square displacement of a walker is proportional to time. The detailed derivation process can refer to Book

[34]. Only considering capillary pores, the classical RWM has been widely used to calculate the effective diffusivity in the cement paste as one-phase-diffusive material [14,35,36]. However, the cement paste studied is two-phase diffusive materials because species can diffuse in capillary pore and C-S-H. Meanwhile, the diffusivities in capillary pore (D_0) and C-S-H ($D_{C\text{-}S\text{-}H}$) hold great difference, normally by 2–4 orders of magnitude. Zhang et al. [11] compared the water diffusivity through the capillary pore to that through the microstructure of cement paste (including the porous C-S-H) using FEM-based simulation in HYMOSTRUC3D. They demonstrated that the diffusivity through the capillary pore is much lower than that through the microstructure of cement paste, and the contribution of C-S-H to diffusivity should be taken into consideration. As a result, the one-phase-diffusive RWM is not suitable for the simulation of diffusivity in hardened cement paste, which may underestimate the diffusivity.

In order to overcome this drawback, a random walk method for the two-component random-diffusive mixture is applied to the 3D voxel-based hardened cement paste. The algorithm is as follows and its flowchart is shown in Fig. 2. In a random walk simulation, the walker is randomly placed in a diffusive voxel, then tries to move from this central voxel to one of the six possible neighbouring voxels. Since there are two types of diffusive voxels in cement paste, the movability of walker is dependent on the diffusivities of central voxel and target voxel. If the central voxel is capillary pore, the target voxel is likely to be non-diffusive phase, capillary pore and C-S-H. As such, the walk probabilities of the walker from capillary pore voxel to non-diffusive phase, capillary pore voxel and C-S-H voxel are 0, 1.0 and $p_{PC} = \frac{2}{1+\frac{D_0}{D_{C-S-H}}}$. For the non-diffusive target voxel the walker still only stays at the central voxel without performing the movement, by contrast for capillary pore target voxel, the walker moves to this target. With respect to C-S-H target voxel, the movement of walker is determined by the comparison between the value of p_{PC} and the random produced value between 0 and 1; if the random value is smaller than p_{PC}, the movement is performed, otherwise the walker stays at the origin. For the situation that the central voxel is C-S-H, the walk probabilities of walker from C-S-H central voxel to non-diffusive phase voxel, capillary pore voxel and C-S-H voxel are 0, p_{PC} and $p_{CC} = \frac{D_{C-S-H}}{D_0}$. If the target voxel is a

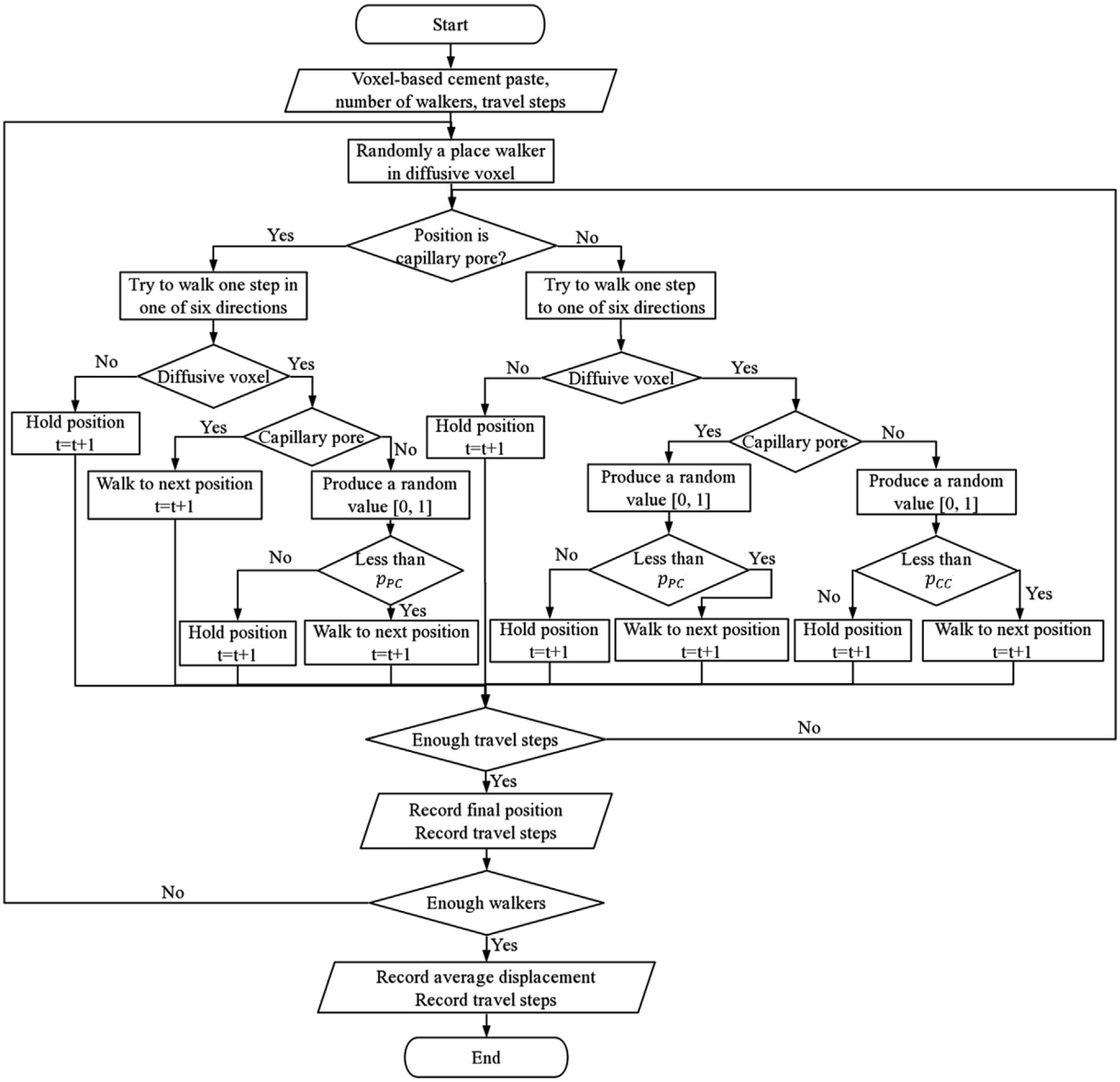

Fig. 2. Flowchart of random walk simulation in hardened cement paste.

non-diffusive phase, the walker will hold the original position. Similar to the movement from capillary pore voxel to C-S-H voxel, as checking the movement of walker from C-S-H towards capillary pore or C-S-H, one random value produced between 0 and 1 is compared to the value of p_{PC} or p_{CC}; if the random value is less than the corresponding walking probability, the walker will move by one step to the next diffusive voxel, otherwise the walker stays at the original position. After attempting to move one step, the travel step increases by 1. After N travel steps (t_N) with a given number of walkers (n), the mean square displacement R_N^2 can be calculated using the following equation

$$\left\langle R_N^2 \right\rangle = \frac{1}{n}\sum_{i=1}^{n}\left[(x_i(t_N)-x_i(0))^2+(y_i(t_N)-y_i(0))^2+(z_i(t_N)-z(0))^2\right] \tag{5}$$

where $x_i(t_N)$ $y_i(t_N)$ and $z_i(t_N)$ are the coordinate of walker i at travel time t_N after N steps, and $x_i(0)$, $y_i(0)$ and $z_i(0)$ are the starting position of walker i. For a larger number of walk steps with sufficient walkers, the curve of $\left\langle R_N^2 \right\rangle$ versus t_N tends to be a straight line. The relative diffusivity in hardened cement paste (D/D_0) equals to the product of the slope of curve and the volume fraction of diffusive phases (V_d, capillary pore plus C-S-H), namely

$$D = D_0 \frac{\left\langle R_N^2 \right\rangle}{t_N} V_d \tag{6}$$

It should be noted that as time elapses, the walkers may go out of the RVEs of cement-based materials due to the limited size of cement paste on the scale of dozens of micrometers with the resolution of 0.5 μm/voxel. This out-leaching problem is undesirable and inevitable. Fortunately, boundary conditions can be introduced to avoid this out-leaching phenomenon. For individual ITZ and BCP there is no periodic boundary condition in z-dimension as shown in Fig. 1. If the periodic boundary conditions are applied on the boundary of RVE, the previously connected pores in z-dimension may be disconnected. This phenomenon is clearly shown in Fig. 3 (a). To overcome this drawback, another boundary condition, i.e., mirror boundary condition, was adopted in this study. As shown in Fig. 3(b), the diffusive phase in cement paste without periodic boundary conditions was still connected as the out-leaching phenomenon occurred. In addition, the tortuosity of diffusive phase in cement paste is equal to the initial one. The random walk simulation for two-component random-diffusive mixture has been programmed using C language.

3.2. Determination of walk probability

As one of the most important input parameters, the walk probability between the central voxel phase and the target voxel phase should be determined in advance. In the hardened cement paste, the species in capillary pores and porous C-S-H are regarded to be diffusive [10,37]. Although the diffusive properties in C-S-H are much lower than that in capillary pore, it will be responsible for the overall diffusivity in hardened cement paste as capillary pore reaches depercolation with cement reaction. The depercolation of capillary pore denotes that the capillary pore is disconnected when capillary porosity is smaller than a threshold value. In order to quantify the value of diffusivity in C-S-H, numerous researchers have made great contributions to this question. Based on the experimental conductivities in hardened cement pastes, the average relative diffusivity in C-S-H is deduced to be 1/400 diffusivity in capillary pores (D_0) reported by Garboczi and Bentz [38], equal to 5.1×10^{-12} m^2/s for the chloride ion using $D_0 = 2.032 \times 10^{-9}$ m^2/s. According to the experimental data and analytical model, Bejaoui and Bary [39,40] reported that tritiated water diffusivity in low-density C-S-H is from 3.4×10^{-12} m^2/s to 9.0×10^{-12} m^2/s and that in high-density C-S-H is between 1.0×10^{-13} m^2/s and 8.3×10^{-13} m^2/s. Based on the resistivity test on cement paste, Liu et al. [41] and Ma et al. [42] both reported that the diffusivity in C-S-H is around 1.60×10^{-11} m^2/s by fitting the experimental data. Recently, our publication [43] demonstrated that the ion diffusivity in C-S-H is dramatically influenced by the electrical double layer at the nano-scale and the estimated chloride diffusivity in C-S-H with 0.24 to 0.36 porosity ranges from 2.0×10^{-13} m^2/s to 8.3×10^{-12} m^2/s on the condition of Zeta-potential with + 10 mV and pore solution with 0.5 mol/L NaCl. In general, the species diffusivity in C-S-H is various that is dependent on the species attributes, e.g., electrical property and valence, and diffusive environment, e.g., species concentration and Zeta-potential. To simplify the simulation in this study, the average chloride diffusivity in C-S-H is adopted because chloride is the major factor of reinforced concrete degradation which is a major concern of durability of reinforced concrete. According to the

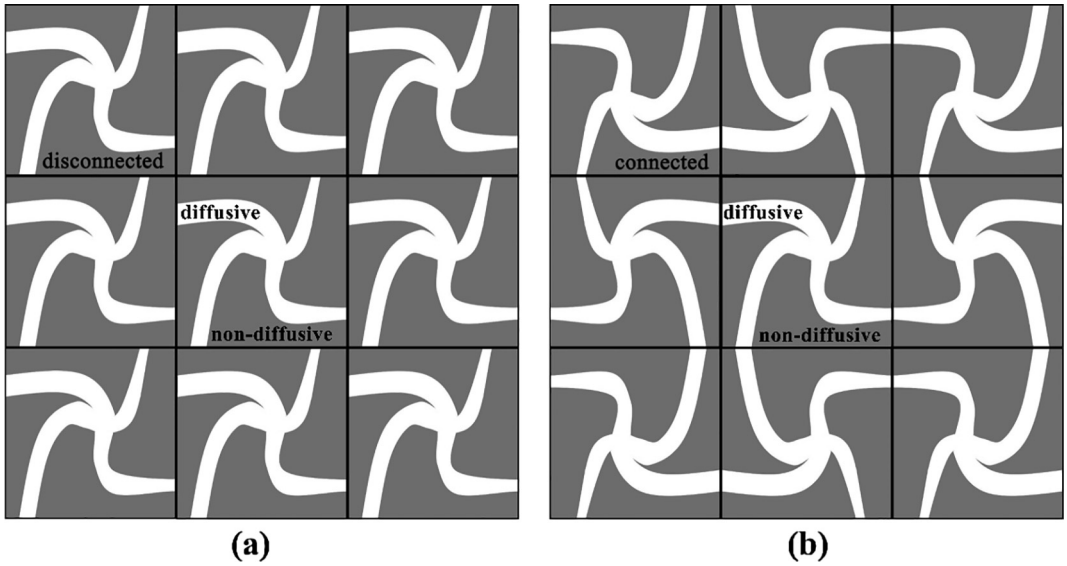

Fig. 3. (a) Periodic boundary conditions; (b) Mirror boundary conditions.

above-mentioned publications, the chloride diffusivity in C-S-H is approximate on the order of 10^{-12} m^2/s. In this study, the average diffusivity in C-S-H was set as 3.0×10^{-12} m^2/s for all simulated cases.

Accordingly, based on the above-mentioned equations, the walk probability moving from the central voxel to the target voxel can be calculated and the results are summarized in Table 1. It can be seen that the walk probability between capillary pores is significantly higher than that between capillary pore and C-S-H, and between C-S-Hs. It is attributed to the lower diffusivity in C-S-H.

4. Results and discussion

4.1. Segmented bulk cement paste and ITZ

Based on the reconstructed pre-hydrated cement pastes between aggregates, the hydration rules are implemented on these discrete microstructures. It should be noted that the volume fractions of cement in the initial packing structures were kept same for the spherical and irregular-shaped cement particles. Herein, the reference w/c ratio of 0.40 as an example is investigated for all cement pastes. The initial packing consisting of irregular-shaped and spherical cement particles are provided in Fig. 4 (top). It can be found that the orientations of the cement particles in the initial packing structure with irregular-shaped particles show randomness, while the distribution of particles is not arbitrary. In the cement paste RVE, the larger particles are away from the rigid boundaries and tend to be located in the middle area of the RVE, which demonstrates the wall effect is well simulated. Meanwhile, the reconstructed prolate cement particles seem to hold fewer probabilities to approach the aggregate surface by contrast to spherical cement due to their geometrical discrepancy.

Table 1
Walk probability moving from central voxel to target voxel.

No.	Central voxel phase	Target voxel phase	Walk probability
1	Capillary pore	Non-diffusive phase	0
2	Capillary pore	Capillary pore	1
3	Capillary pore	C-S-H	0.003
4	C-S-H	Non-diffusive phase	0
5	C-S-H	Capillary pore	0.003
6	C-S-H	C-S-H	0.00148

$D_0 = 2.032 \times 10^{-9}$ m^2/s, $D_{C\text{-}S\text{-}H} = 3.0 \times 10^{-12}$ m^2/s.

As cement hydration proceeds, the cement particles continuously dissolve and hydration products correspondingly produce. The microstructures of hydrated cement pastes with the degree of hydration of 0.8 (equal to curing 28 d) are shown in Fig. 4 (bottom). Although the surface area of cement particles has a strong effect on the hydration kinetics [17], for CEMHYD3D model, the simulated hydration process for different shaped cement particles related to the real time (t) can be adjusted by the following equation

$$t = \beta n^2 \tag{7}$$

where β is the conversion factor and n is the computational cycle [27,28]. To compare the effect of morphological difference on microstructural development, we only use the degree of hydration as the judgment criteria for all microstructures in this study regardless of the difference of surface area. From the two hydrated cement pastes, in addition to the capillary pores and unhydrated cement observed above, hydration products in cement pastes between aggregates are also consistent with the experimental phenomenon [20]. For example, calcium hydroxide (blue) tends to accumulate near the aggregate surfaces within a small thickness by contrast to other hydration products, e.g., C-S-H, is barren in this area.

To investigate the difference of diffusive properties between ITZ and BCP, cement paste is artificially separated into these two parts. Although some noticeable breakthroughs of the structure of ITZ have been achieved, this area is not still fully understood and needs to be investigated. For the transport property, it highly depends on the capillary pore structures in hardened cement pastes [16]. Likewise, the distribution of cement particles also plays an important role in pore structures in cement pastes. As a result, we attach great importance on the distributions of capillary pores and unhydrated cement in cement pastes between aggregates for the separation of ITZ and BCP, and comparison of different cement pastes, which is similar to other modelling cases [24,44–48]. The statistical porosities in pre-hydrated and hydrated cement pastes away from the aggregate surface are shown in Fig. 5(a). Herein, it should be noted that ten parallel simulated samples are adopted in this study. We can see that in spite of the local disorder in particle packing, e.g., the area around 20 μm, the changing tendencies of average capillary porosities with irregular-shaped and spherical

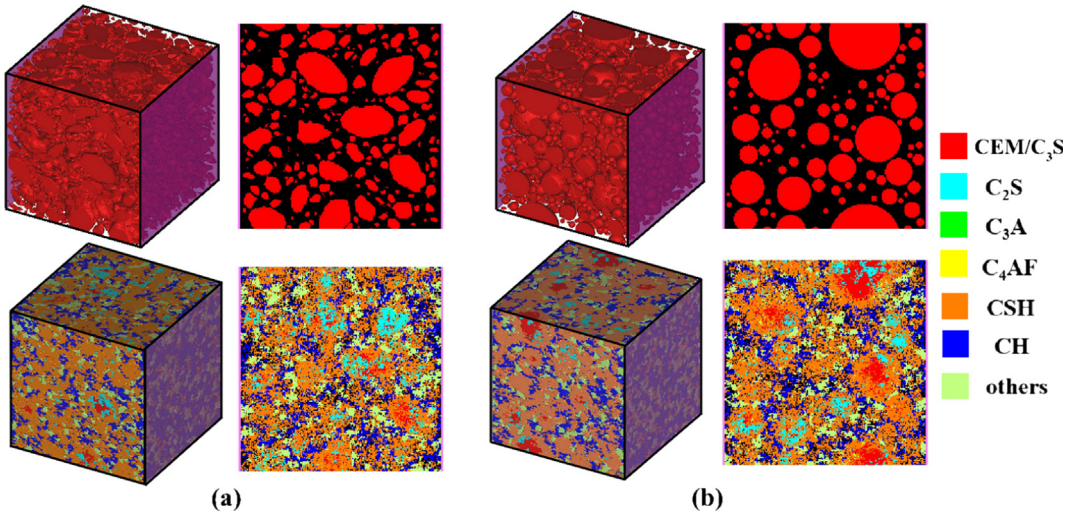

Fig. 4. Initial packing and hydrated microstructures of cement particles consisting of irregular-shaped and spherical particles (purple – aggregate surface). The degree of hydrations in hydrated cement pastes are both 0.8 corresponding to curing 28 days. (For interpretation of the references to colour in this figure legend, the reader is referred to the web version of this article.)

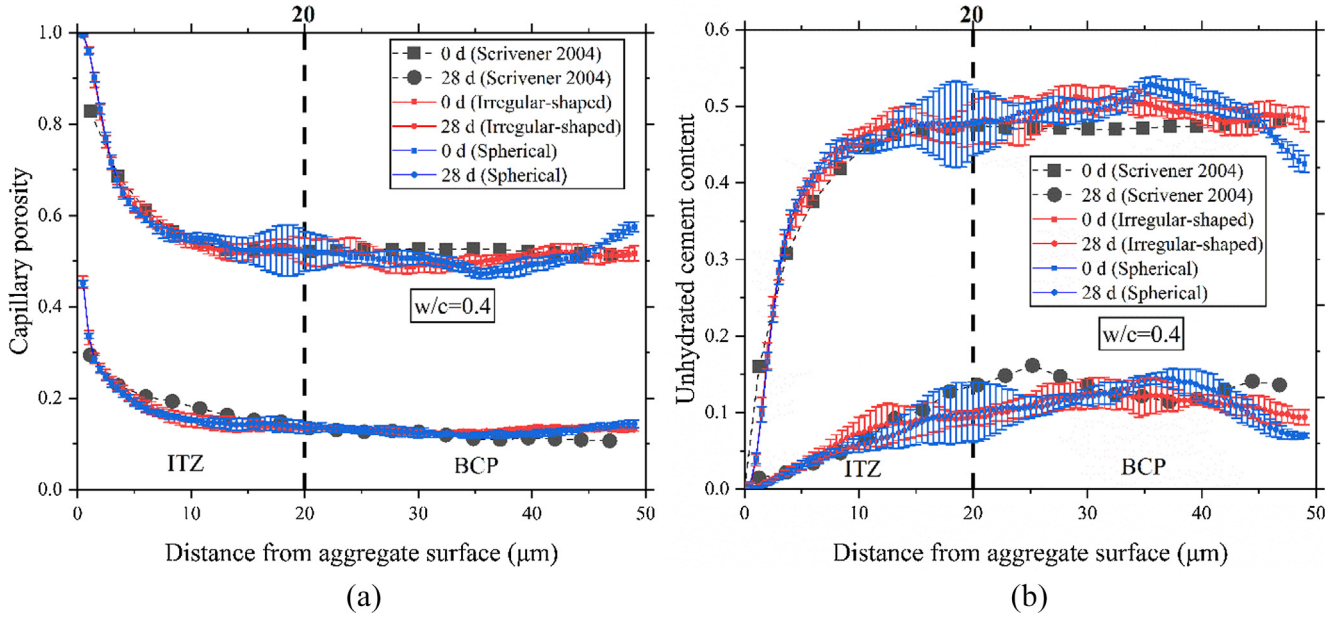

Fig. 5. Simulated and experimental porosity distributions (a) and unhydrated cement contents (b) in cement pastes between aggregates away from the aggregate surface.

particles are similar. The observed results in this study agree well with that from Xu et al. [49]. In their study, the outcomes demonstrate that the changing tendencies of capillary porosities in pre-hydrated cement pastes between aggregates are independent on the shapes of cement particles when the shapes of cement particles are simplified as ellipsoids. As cement hydration proceeds, the porosities become decreasing and their difference in each sample tends to stable within a small range. It means that with DOH increasing, the effect of cement particle shapes on the distribution of capillary porosity becomes weaker. Furthermore, it is interesting to find that the simulated results both fit well with the experimental data from Ref. [20]. Correspondingly, the changing tendencies of the content of unhydrated cement in cement pastes consisting of irregular-shaped and spherical particles are shown in Fig. 5(b). Similar to the observed outcomes of capillary porosities, the shapes of cement particles also have a slight effect on the contents of unhydrated cement away from the aggregate surface. In addition, the results from the simulation are overall consistent with the experimental data.

After obtaining the quantitative distribution of representative phases, the ITZ structure with an exact thickness can be extracted. Fig. 6 shows an example in which the cement paste can be divided into two symmetrical sections. However, the determination of the thickness of ITZ is far from being a trivial task because the structure and thickness of ITZ change with curing time, w/c ratio and raw materials [29]. In addition, the criteria for separation is non-uniform and even arbitrary [25]. To reduce the difficulty of modelling procedures, most models adopt the ITZ with a constant thickness without changing with curing time [24,44–48]. Therefore, combined with the observed results from Fig. 5, the selected thicknesses of ITZ and BCP are determined to be 20 μm and 30 μm respectively for the all simulated cement pastes.

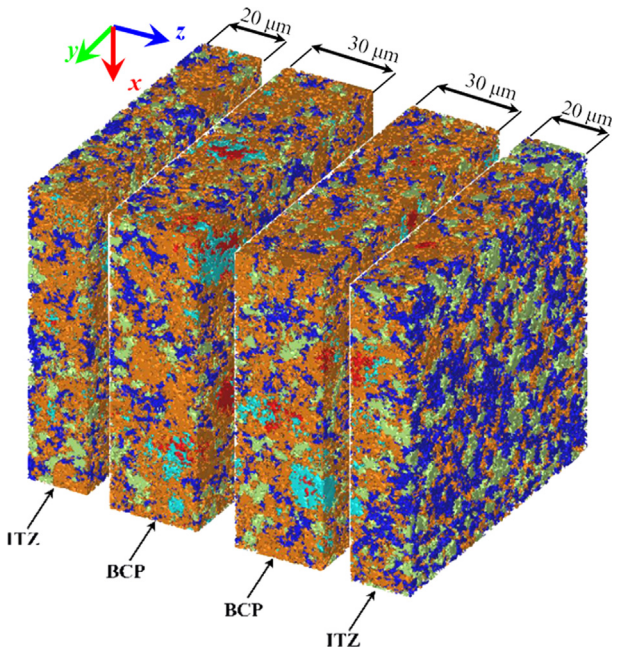

Fig. 6. Separation of ITZ and BCP at 28 days.

4.2. Validation of RWM

After determining the microstructures of BCP and ITZ, the proposed RWM is applied to them. Since RWM is a statistic approach, the linear relationship between mean squared displacement of walkers and travel steps is correct only under the conditions of a large number of walkers and travel steps. As a result, the number of walkers and travel steps used should be determined in advance. Herein, two cement pastes simulated using spherical cement powders (DOH = 0.50 and 0.85 at a 0.40 w/c ratio) are employed as examples. The average squared displacements versus travel steps in BCP and ITZ are respectively investigated. The curves between average squared displacement and number of walk steps (from 5 walkers to 500,000 walkers) are plotted in Fig. 7. In the cement paste with a 0.50 DOH shown in Fig. 7(a), it can be seen that as the number of walker reaches 5000, the curves tend to be linear lines for BCP and ITZ. In addition, the slope of ITZ is greater than that of BCP which is attributed to the higher capillary porosity in ITZ compared to BCP. Similarly, in terms of the cement paste with a 0.85 DOH shown in Fig. 7(b), as the number of walker reaches 50000, the average squared displacement increases linearly with

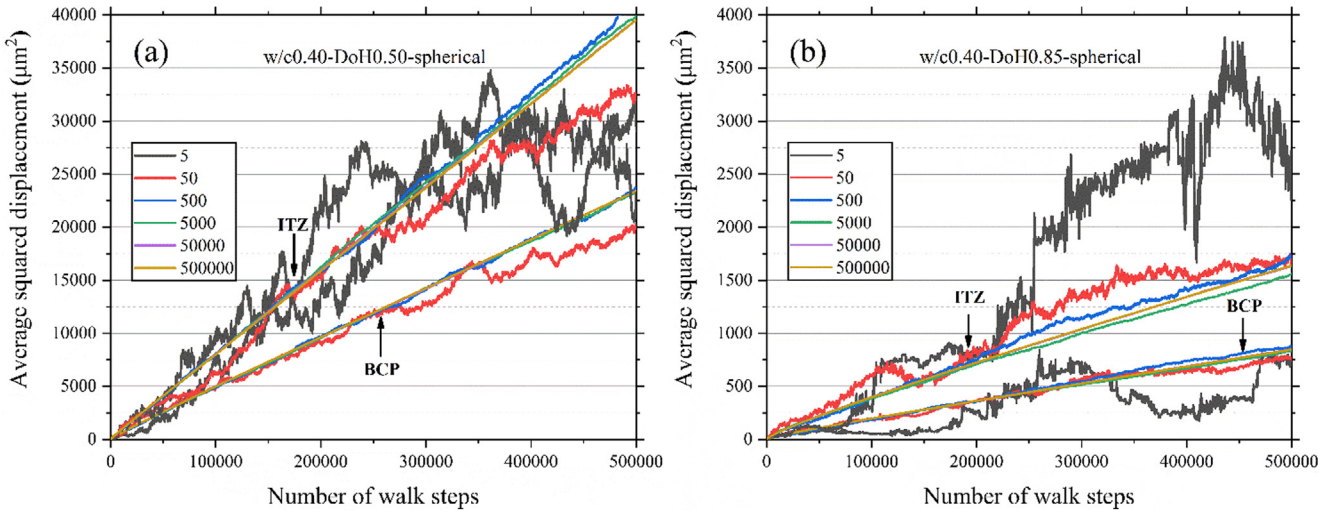

Fig. 7. Effect of the number of walk steps and walkers on the average squared displacement in hardened cement pastes (BCP and ITZ) at a 0.40 w/c ratio with 0.50 and 0.85 DOHs using spherical cement powders.

the travel steps. Additionally, compared to the cement paste with a 0.50 DOH, the mean squared displacement in the cement paste with a 0.85 DOH is much lower. It is ascribed to the fact that the cement paste with a lower DOH holds higher capillary porosity which leads to larger walk probability of walker. According to the modelling results from these two cases, as the number of walker reaches 50000, the curve of mean squared displacement versus the number of walk step shows a good linear relationship. To determine the effect of the number of walk steps, the relationship between the slope and the number of walk step is plotted in Fig. 8. As can been seen, the cement paste with a 0.85 DOH needs more walker steps to reach a stable slope, compared to that with a 0.50 DOH. Nevertheless, as the number of walk steps exceeds 30,000, the slopes all show stable values with sufficient walker, i.e., 50,000. As a result, according to the modelling results from these two cases, the number of walkers and travel steps are selected as 50,000 and 500,000 in all simulation cases in this study.

4.3. Diffusivity prediction

The simulated average diffusivities in cement pastes at 0.30, 0.40 and 0.50 w/c ratios are shown in Fig. 9. Herein, twenty sets of BCP and ITZ were used to decrease the statistic error. It is indicated in Fig. 9 that with DOH increasing, the diffusivities decrease generally from 10^{-9} to 10^{-12} m^2/s for BCPs and ITZs at w/c ratios of 0.30, 0.40 and 0.50. This is ascribed to the fact that the hydration products fill the capillary pore which leading to the decreasing capillary porosity and the more tortuous capillary pore structure. In addition, the diffusivity in ITZ is consistently higher than that in BCP, which is due to the higher capillary porosity in ITZ. In terms of the shaped discrepancy of cement powders, the diffusivity in cement paste simulated using spherical cement powder is slightly higher than that simulated using irregular-shaped one. The contrast ratios of diffusivities between spherical and irregular-shaped cement powders (D_s/D_r) holds 0–40%. Although using the spherical cement powder is likely to overestimate the diffusivity in cement paste, the error is still acceptable compared to the large difference of diffusivity with cement hydration, i.e., normally two orders of magnitude difference.

The overestimated diffusivity for spherical cement powders can be attributed to three discrepancies, i.e., initial packing of cement powder, capillary pore structure, and C-S-H morphology. Firstly, in the initial packing of cement powder shown in Fig. 9, the diffusivity in cement paste simulated using spherical cement demonstrates 5%-10% higher than that using irregular-shaped cement. Since the irregular-shaped cement is more irregular than spherical

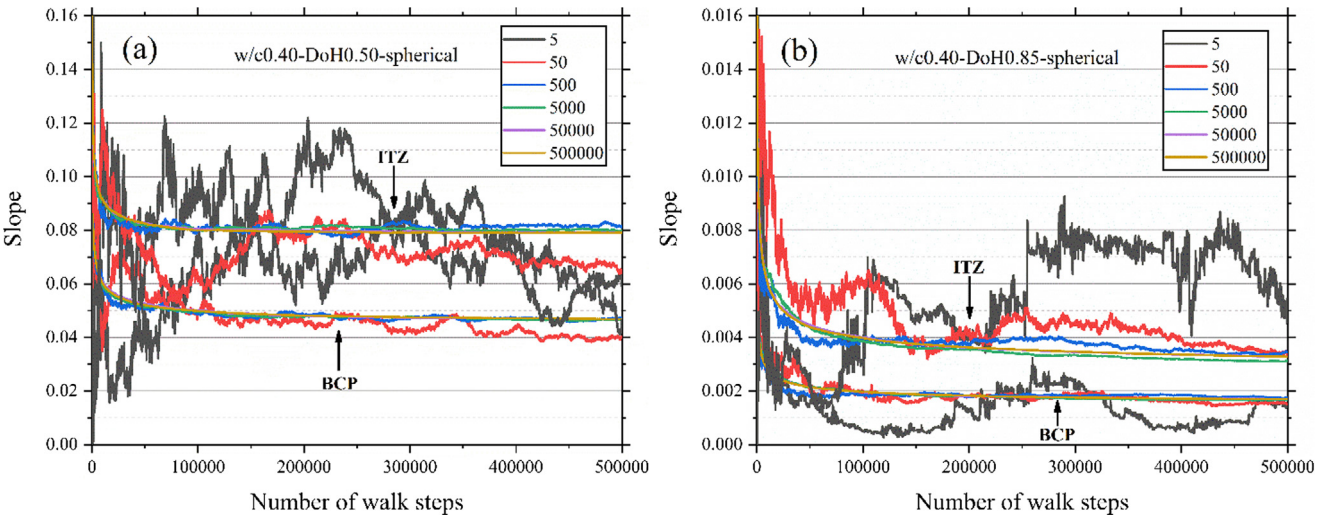

Fig. 8. Effect of the number of walk steps and walkers on the slope of the average squared displacement versus the number of walk steps.

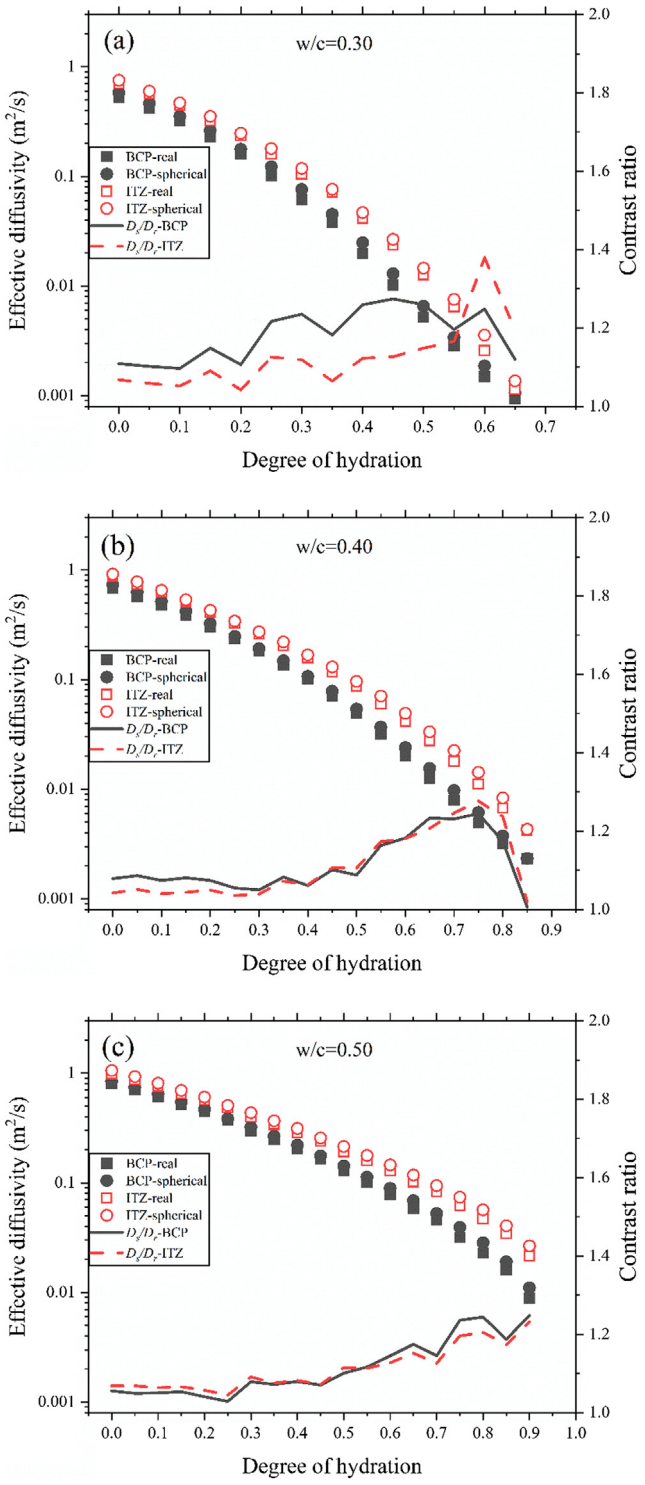

Fig. 9. Predicted diffusivity in hardened cement paste simulated by irregular-shaped and spherical cement powders. (D_r and D_s denote the diffusivities simulated using irregular-shaped and spherical cement powders).

cement, the diffusion tortuosity in pre-hydrated cement paste simulated using spherical cement is lower than that using irregular-shaped cement. This finding is consistent with that from Abyaneh et al. [50]. In their study, the diffusivity in the mortar was simulated using several ellipsoidal sands and the conclusion shows that for the well-curing mortars with same sand volume fraction, the diffusivity in mortar increase with the increasing length-to-diameter ratios.

Secondly, as cement hydration proceeds, the degree of overestimation of diffusivity becomes more significant. As shown in Fig. 9, in the cement pastes at w/c ratios of 0.30 and 0.40. The overestimated diffusivities grow from 5–10% to 20–40% as DOH increasing to 0.6 for 0.30 w/c ratio and 0.75 for 0.40 w/c ratio. And the degree of overestimated diffusivity in cement paste at a 0.50 w/c ratio consistently increases with the increasing DOH. This phenomenon can be confirmed using the change of tortuosity and connectivity of capillary pore in cement paste with DOH. Herein, the tortuosity of the capillary pore can be also determined using RWM where the walkers are randomly placed and only walk in the capillary pore voxels [16]. Combined with the square displacement $\langle R_N^2 \rangle$ expressed in Eq. (5), the diffusion tortuosity of capillary pore (τ_D) can be expressed as

$$\tau_D = \frac{\langle R_N^2 \rangle}{t_N} \tag{8}$$

Therefore, similar to the previous input parameters, the number of walkers and travel steps are selected as 50,000 and 500,000 in all simulation cases in this study. As an example, the diffusion tortuosity versus DOH in the cement pastes at a 0.4 w/c ratio is plotted in Fig. 10. It is observed that the diffusion tortuosity in cement paste simulated using irregular-shaped cement increase is slightly higher than that using spherical cement, which leads to the lower diffusivity for spherical cement with DOH. In Fig. 10, it can be found that some values of diffusion tortuosity are absent, which means the capillary pores are disconnected and the diffusive channel becomes dependent on the C-S-H path.

In terms of the connectivity of capillary pore, to quantitatively link the predicting difference of diffusivity with the connectivity of capillary pore, the connectivity of capillary pore in the hydrating cement paste was determined using burning algorithm [51]. As a representative example, the cement paste with a 0.4 w/c ratio was selected because the capillary pore at this w/c ratio experiences the depercolation, as shown in Fig. 10. The relationship between the connectivity of capillary pore and D_s/D_r is indicated in Fig. 11. It can be found that the depercolation of the capillary pore in cement paste simulated using irregular-shaped cement particles is prior to that simulated using spherical cement particles, which is ascribed to the geometric effect of cement particles [17]. Meanwhile, the connectivity of capillary pore holds a large difference in the vicinity of the depercolation of capillary pore, i.e.,

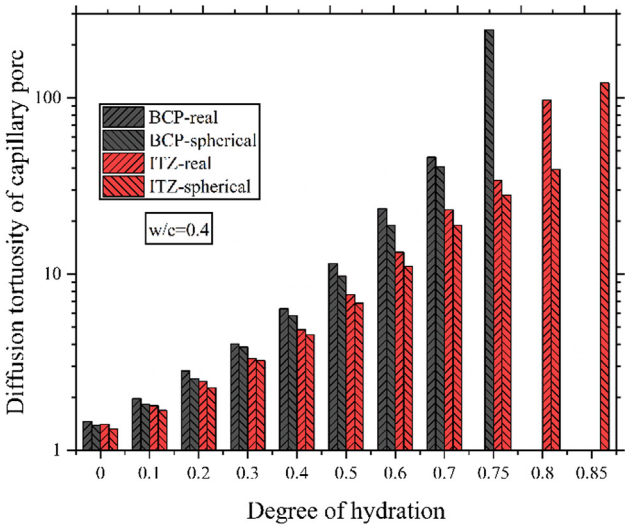

Fig. 10. Diffusion tortuosity in cement paste at a 0.40 w/c ratio.

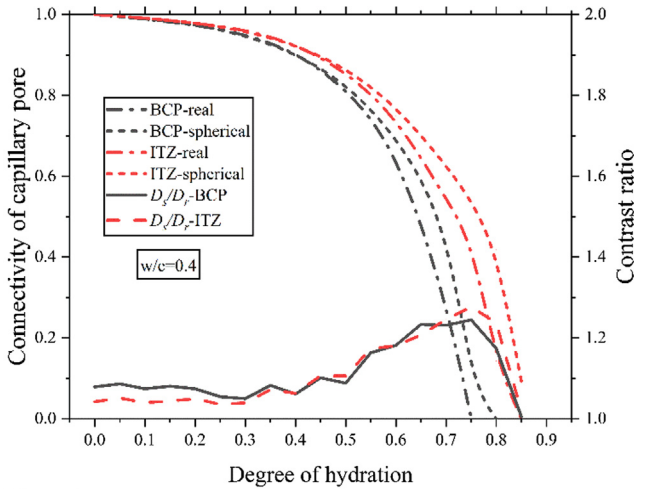

Fig. 11. Relationship between connectivity of capillary pore and contrast ratio of diffusivities simulated using spherical and irregular-shaped cement particles in cement paste at a 0.40 w/c ratio.

between 0.60 and 0.85 DOH. In terms of the relationship between the connectivity of capillary pore and D_s/D_r, it is interesting to find that the maximum D_s/D_r is located in this range of DOH.

Finally, as the cement hydration proceeds, more and more capillary pores are disconnected. As capillary pores reach the depercolation, the C-S-H paths become the diffusive channels. With cement hydrating and hydration products forming, the initial shape of cement particles become increasingly lost. This loss of shape information is expected because hydration proceeds by surface reactions (dissolution of unhydrated cement and growth of hydration products). The morphology of C-S-H formed is dependent on the shape of cement particles. For the high w/c ratios, e.g., 0.4 and 0.5, since most cement particles have been consumed at the later curing age, the effect of the initial shape of cement powders on the morphology of C-S-H is weaker, which can be demonstrated in Fig. 4. The unhydrated cement particles in hydrated cement pastes at the later curing age both tend to be spherical. There is no obvious difference in the microstructure of hydrated cement pastes using irregular-shaped and spherical cement powders at the later curing age. The similar microstructures of cement pastes simulated irregular-shaped and spherical particles leads to the similar predicting diffusivities. As can be seen in Fig. 9(b), the D_s/D_r ratios for BCP and ITZ both tend to be 1.0 at a w/c ratio of 0.4 with a DOH of 0.85. However, for the low w/c ratios, e.g., 0.3, the DOH of medium and larger cement particles is low. The shape of medium and larger cement particles can be still distinguished. These unhydated cement particles lead to the morphology of C-S-H with a similar shape to the unhydated cement particles, which increases the predicting error of diffusivity for the spherical particles. As can be seen in Fig. 10(a), D_s/D_r ratios at a w/c ratio of 0.3 are still large even at the later curing age, e.g., 1.22 for BCP and 1.40 for ITZ with a DOH of 0.60. Therefore, the effect of the formation of C-S-H morphology becomes significant with the w/c ratio decreasing.

5. Concluding remarks

In this study, a microstructure-based model is presented to simulate the hydrating cement pastes between aggregates and predict their effective diffusivity. To assess the effect of initial shape of cement powder shapes on the microstructural formation of simulated cement paste and on the predicted effective diffusivity in cement paste, two case studies are investigated, i.e., using spherical cement powder and irregular-shaped cement powder that is close to the real cement powder. The results are indicated as follows:

- The effect of the shape of cement powders on the distributions of capillary pore and unhydrated cement is weak. Meanwhile, the volume fractions of capillary pore and unhydrated cement particles in simulated cement pastes between aggregates away from aggregate surface agree well with the measured results.
- A random walk method for the two-component random-diffusive mixture is proposed to apply to the 3D voxel-based hardened cement paste. The predicting diffusivity is correct only under the conditions of a large number of travel steps and walkers. In this study, the number of walkers and travel steps are set as 50,000 and 500,000, which are sufficient to obtain the good linear relationship between the mean square displacement and number of travel steps.
- Compared to the irregular-shaped cement powders that are close to the real one, the diffusivity in cement paste simulated using spherical cement powders is overestimated by 0–40%. It is ascribed to three discrepancies, i.e., the shape of initial cement powder, the formation of capillary pore structure, and the formation of C-S-H structure.
- In the initial packing of cement powders, the diffusivity in cement paste simulated using spherical cement demonstrates 5%-10% higher than that using irregular-shaped cement.
- The difference of capillary pore structure induced by the shaped discrepancy of initial cement particles is divided into two aspects, i.e., tortuosity and connectivity of capillary pore. The capillary pore in cement paste simulated using spherical particles shows lower tortuosity and higher connectivity by contrast to that simulated using irregular-shaped particles.
- The difference of C-S-H morphology induced by the shaped discrepancy of initial cement particles is w/c ratio-dependent. This effect becomes significant with the w/c ratio decreasing.

Declaration of Competing Interest

No conflict of interest.

Acknowledgments

The financial support from National Key Research and Development Program of China (NO. 2018YFC0705400), National Natural Science Foundation of China (No. 51778613 and NO. 51678143) and Ministry of Science and Technology of China (973 Program, No. 2015CB655102) are gratefully acknowledged.

References

[1] D. Crete, General guidelines for durability design and redesign, The European Union-Brite Eu Ram III, Project No. BE95-1347:'Probabilistic Performance Based Durability Design of Concrete Structures', Document, 15 (2000).
[2] R.A. Patel, Q.T. Phung, S.C. Seetharam, J. Perko, D. Jacques, N. Maes, G. De Schutter, G. Ye, K. Van Breugel, Diffusivity of saturated ordinary Portland cement-based materials: a critical review of experimental and analytical modelling approaches, Cem. Concr. Res. 90 (2016) 52–72.
[3] C.F. Dunant, B. Bary, A.B. Giorla, C. Péniguel, J. Sanahuja, C. Toulemonde, A.-B. Tran, F. Willot, J. Yvonnet, A critical comparison of several numerical methods for computing effective properties of highly heterogeneous materials, Adv. Eng. Softw. 58 (2013) 1–12.
[4] M.I. Idiart, F. Willot, Y.-P. Pellegrini, P.P. Castaneda, Infinite-contrast periodic composites with strongly nonlinear behavior: Effective-medium theory versus full-field simulations, Int. J. Solids Struct. 46 (2009) 3365–3382.
[5] S. Das, A. Maroli, S.S. Singh, T. Stannard, X. Xiao, N. Chawla, N. Neithalath, A microstructure-guided constitutive modeling approach for random heterogeneous materials: application to structural binders, Comput. Mater. Sci. 119 (2016) 52–64.

[6] D.P. Bentz, D.P. Bentz, CEMHYD3D: A Three-Dimensional Cement Hydration and Microstructure Development Modelling Package. Version 2.0, US Department of Commerce, National Institute of Standards and Technology, 2000.
[7] K. Van Breugel, Simulation of hydration and formation of structure in hardening cement-based materials, (1993).
[8] E. Garboczi, D. Bentz, Computer simulation of the diffusivity of cement-based materials, J. Mater. Sci. 27 (1992) 2083–2092.
[9] S. Kamali-Bernard, F. Bernard, W. Prince, Computer modelling of tritiated water diffusion test for cement based materials, Comput. Mater. Sci. 45 (2009) 528–535.
[10] Y. Yang, M. Wang, Pore-scale modeling of chloride ion diffusion in cement microstructures, Cem. Concr. Compos. 85 (2018) 92–104.
[11] M. Zhang, G. Ye, K. Van Breugel, Microstructure-based modeling of water diffusivity in cement paste, Constr. Build. Mater. 25 (2011) 2046–2052.
[12] M. Zhang, G. Ye, K. van Breugel, Modeling of ionic diffusivity in non-saturated cement-based materials using lattice Boltzmann method, Cem. Concr. Res. 42 (2012) 1524–1533.
[13] N. Ukrainczyk, E. Koenders, Representative elementary volumes for 3D modeling of mass transport in cementitious materials, Modell. Simul. Mater. Sci. Eng. 22 (2014) 035001.
[14] L. Liu, W. Sun, G. Ye, H. Chen, Z. Qian, Estimation of the ionic diffusivity of virtual cement paste by random walk algorithm, Constr. Build. Mater. 28 (2012) 405–413.
[15] C. Liu, R. Huang, Y. Zhang, Z. Liu, M. Zhang, Modelling of irregular-shaped cement particles and microstructural development of Portland cement, Constr. Build. Mater. 168 (2018) 362–378.
[16] C. Liu, G. Liu, Z. Liu, L. Yang, M. Zhang, Y. Zhang, Numerical simulation of the effect of cement particle shapes on capillary pore structures in hardened cement pastes, Constr. Build. Mater. 173 (2018) 615–628.
[17] J.W. Bullard, E.J. Garboczi, A model investigation of the influence of particle shape on portland cement hydration, Cem. Concr. Res. 36 (2006) 1007–1015.
[18] H. Chen, Z. Zhu, J. Lin, W. Xu, L. Liu, Numerical modeling on the influence of particle shape on ITZ's microstructure and macro-properties of cementitious composites: a critical review, J. Sustainable Cement-Based Mater. 7 (2018) 248–269.
[19] R.A. Patel, J. Perko, D. Jacques, G. De Schutter, G. Ye, K. Van Bruegel, Effective diffusivity of cement pastes from virtual microstructures: role of gel porosity and capillary pore percolation, Constr. Build. Mater. 165 (2018) 833–845.
[20] K.L. Scrivener, A.K. Crumbie, P. Laugesen, The interfacial transition zone (ITZ) between cement paste and aggregate in concrete, Interface Sci. 12 (2004) 411–421.
[21] M. Zhang, G. Ye, K. van Breugel, Multiscale lattice Boltzmann-finite element modelling of chloride diffusivity in cementitious materials. Part I: algorithms and implementation, Mech. Res. Commun. 58 (2014) 53–63.
[22] N.L. Le, M. Stroeven, L.J. Sluys, P. Stroeven, A novel numerical multi-component model for simulating hydration of cement, Comput. Mater. Sci. 78 (2013) 12–21.
[23] K. Li, P. Stroeven, M. Stroeven, L.J. Sluys, A numerical investigation into the influence of the interfacial transition zone on the permeability of partially saturated cement paste between aggregate surfaces, Cem. Concr. Res. 102 (2017) 99–108.
[24] D.P. Bentz, E.J. Garboczi, C.J. Haecker, O.M. Jensen, Effects of cement particle size distribution on performance properties of Portland cement-based materials, Cem. Concr. Res. 29 (1999) 1663–1671.
[25] P. Carrara, L. De Lorenzis, Consistent identification of the interfacial transition zone in simulated cement microstructures, Cem. Concr. Compos. 80 (2017) 224–234.
[26] E.J. Garboczi, D.P. Bentz, The effect of statistical fluctuation, finite size error, and digital resolution on the phase percolation and transport properties of the NIST cement hydration model, Cem. Concr. Res. 31 (2001) 1501–1514.
[27] D.P. Bentz, A three-dimensional cement hydration and microstructure program: I. Hydration rate, heat of hydration, and chemical shrinkage, Build. Fire Res. Lab., Nat. Inst. Technol. (1995).
[28] D.P. Bentz, Three-dimensional computer simulation of Portland cement hydration and microstructure development, J. Am. Ceram. Soc. 80 (1997) 3–21.
[29] Y. Gao, G. De Schutter, G. Ye, Micro-and meso-scale pore structure in mortar in relation to aggregate content, Cem. Concr. Res. 52 (2013) 149–160.
[30] S. Diamond, J. Huang, The ITZ in concrete–a different view based on image analysis and SEM observations, Cem. Concr. Compos. 23 (2001) 179–188.
[31] C. Liu, R. Qian, Z. Liu, Y. Zhang, M. Zhang, Shape analysis of cement powder and supplementary cementitious materials using high-resolution X-ray computed tomography, Submitted to Powder Technology.
[32] L. Holzer, R.J. Flatt, S.T. Erdoğan, J.W. Bullard, E.J. Garboczi, Shape comparison between 0.4–2.0 and 20–60 μm cement particles, J. Am. Ceram. Soc. 93 (2010) 1626–1633.
[33] E.J. Garboczi, J.W. Bullard, Shape analysis of a reference cement, Cem. Concr. Res. 34 (2004) 1933–1937.
[34] B.D. Hughes, Random walks and random environments, (1995).
[35] M.A.B. Promentilla, T. Sugiyama, T. Hitomi, N. Takeda, Quantification of tortuosity in hardened cement pastes using synchrotron-based X-ray computed microtomography, Cem. Concr. Res. 39 (2009) 548–557.
[36] H. Ma, D. Hou, Z. Li, Two-scale modeling of transport properties of cement paste: Formation factor, electrical conductivity and chloride diffusivity, Comput. Mater. Sci. 110 (2015) 270–280.
[37] R.A. Patel, J. Perko, D. Jacques, G. De Schutter, G. Ye, K. Van Breugel, A three-dimensional lattice Boltzmann method based reactive transport model to simulate changes in cement paste microstructure due to calcium leaching, Constr. Build. Mater. 166 (2018) 158–170.
[38] E. Garboczi, D. Bentz, Modelling of the microstructure and transport properties of concrete, Constr. Build. Mater. 10 (1996) 293–300.
[39] S. Bejaoui, B. Bary, Modeling of the link between microstructure and effective diffusivity of cement pastes using a simplified composite model, Cem. Concr. Res. 37 (2007) 469–480.
[40] B. Bary, S. Béjaoui, Assessment of diffusive and mechanical properties of hardened cement pastes using a multi-coated sphere assemblage model, Cem. Concr. Res. 36 (2006) 245–258.
[41] Z. Liu, Y. Zhang, L. Liu, Q. Jiang, An analytical model for determining the relative electrical resistivity of cement paste and C-S–H gel, Constr. Build. Mater. 48 (2013) 647–655.
[42] H. Ma, D. Hou, J. Liu, Z. Li, Estimate the relative electrical conductivity of C-S–H gel from experimental results, Constr. Build. Mater. 71 (2014) 392–396.
[43] Y. Zhang, C. Liu, Z. Liu, G. Liu, L. Yang, Modelling of diffusion behavior of ions in low-density and high-density calcium silicate hydrate, Constr. Build. Mater. 155 (2017) 965–980.
[44] J.D. Shane, T.O. Mason, H.M. Jennings, E.J. Garboczi, D.P. Bentz, Effect of the interfacial transition zone on the conductivity of Portland cement mortars, J. Am. Ceram. Soc. 83 (2000) 1137–1144.
[45] Z. Sun, E.J. Garboczi, S.P. Shah, Modeling the elastic properties of concrete composites: Experiment, differential effective medium theory, and numerical simulation, Cem. Concr. Compos. 29 (2007) 22–38.
[46] P. Stroeven, M. Stroeven, Reconstructions by SPACE of the interfacial transition zone, Cem. Concr. Compos. 23 (2001) 189–200.
[47] Y. Gao, G. De Schutter, G. Ye, H. Huang, Z. Tan, K. Wu, Characterization of ITZ in ternary blended cementitious composites: experiment and simulation, Constr. Build. Mater. 41 (2013) 742–750.
[48] Z. Liu, W. Chen, Y. Zhang, H. Lv, A three-dimensional multi-scale method to simulate the ion transport behavior of cement-based materials, Constr. Build. Mater. 120 (2016) 494–503.
[49] W. Xu, H. Chen, Microstructural characterization of fresh cement paste via random packing of ellipsoidal cement particles, Mater. Charact. 66 (2012) 16–23.
[50] S.D. Abyaneh, H. Wong, N. Buenfeld, Modelling the diffusivity of mortar and concrete using a three-dimensional mesostructure with several aggregate shapes, Comput. Mater. Sci. 78 (2013) 63–73.
[51] D.P. Bentz, E.J. Garboczi, Percolation of phases in a three-dimensional cement paste microstructural model, Cem. Concr. Res. 21 (1991) 325–344.